Single vacancy defect spectroscopy on HfO_2 using random telegraph noise signals from scanning tunneling microscopy

R. Thamankar', N. Raghavan, J. Molina, F. M. Puglisi, S. J. O'Shea, K. Shubhakar, L. Larcher, P. Pavan, A. Padovani, and K. L. Pey

Citation: J. Appl. Phys. **119**, 084304 (2016); doi: 10.1063/1.4941697
View online: http://dx.doi.org/10.1063/1.4941697
View Table of Contents: http://aip.scitation.org/toc/jap/119/8
Published by the American Institute of Physics

JOURNAL OF APPLIED PHYSICS **119**, 084304 (2016)

Single vacancy defect spectroscopy on HfO_2 using random telegraph noise signals from scanning tunneling microscopy

R. Thamankar,[1,a)] N. Raghavan,[1] J. Molina,[2] F. M. Puglisi,[3] S. J. O'Shea,[4] K. Shubhakar,[1] L. Larcher,[5,6] P. Pavan,[3] A. Padovani,[6] and K. L. Pey[1]
[1]*Singapore University of Technology and Design (SUTD), 8 Somapah Road, Singapore 487372*
[2]*National Institute of Astrophysics, Optics and Electronics, Tonantzintla, Puebla, Mexico*
[3]*DIEF—Università di Modena e Reggio Emilia, Via P. Vivarelli 10/1, 41125 Modena, Italy*
[4]*A*STAR Institute of Materials Research and Engineering (IMRE), 2 Fusionopolis Way, Singapore 138634*
[5]*DISMI—Università di Modena e Reggio Emilia, 42122 Reggio Emilia, Italy*
[6]*MDLab s.r.l., Loc. Grand Chemin 30, 11020 Saint Christophe, Aosta, Italy*

(Received 24 September 2015; accepted 20 January 2016; published online 25 February 2016)

Random telegraph noise (RTN) measurements are typically carried out at the device level using standard probe station based electrical characterization setup, where the measured current represents a cumulative effect of the simultaneous response of electron capture/emission events at multiple oxygen vacancy defect (trap) sites. To better characterize the individual defects in the high-κ dielectric thin film, we propose and demonstrate here the measurement and analysis of RTN at the nanoscale using a room temperature scanning tunneling microscope setup, with an effective area of interaction of the probe tip that is as small as 10 nm in diameter. Two-level and multi-level RTN signals due to single and multiple defect locations (possibly dispersed in space and energy) are observed on 4 nm HfO_2 thin films deposited on *n*-Si (100) substrate. The RTN signals are statistically analyzed using the Factorial Hidden Markov Model technique to decode the noise contribution of more than one defect (if any) and estimate the statistical parameters of each RTN signal (i.e., amplitude of fluctuation, capture and emission time constants). Observation of RTN at the nanoscale presents a new opportunity for studies on defect chemistry, single-defect kinetics and their stochastics in thin film dielectric materials. This method allows us to characterize the fast traps with time constants ranging in the millisecond to tens of seconds range. © *2016 AIP Publishing LLC*. [http://dx.doi.org/10.1063/1.4941697]

I. INTRODUCTION

Oxygen vacancy defects are known to be the predominant precursors for degradation and breakdown in ultra-thin dielectric logic devices.[1,2] With the aggressive scaling of complementary metal oxide semiconductor (CMOS) technology towards the 14 nm and 10 nm nodes, the role of discrete individual process-induced defects/traps (PITs) will be more detrimental both in terms of serving as a weak link for degradation and causing eventual percolation-assisted breakdown. One of the widely adopted approaches to study the defect chemistry and energetics is to bias the transistor gate terminal at a low voltage condition for a moderately long duration of time to detect random telegraph noise (RTN) signals in the gate current (I_g) that arise due to the stochastic random electron capture/emission events at the defect sites (traps).[3,4] The I_g-RTN signals measured over time appear as stochastic digital fluctuations amongst discrete conduction levels. In general, the electron deactivates a defect when it gets captured reducing the trap-assisted tunneling conductivity and activates it when the electron is emitted,[5] resulting in a reversible digital shift in conductivity between two levels for a single trap. In the simplest case, the measured RTN signal only displays two discrete current levels (2-level RTN) associated with capture/emission at a single defect site.[6] The amount of time spent by the signal in each discrete level before a transition occurs is exponentially distributed,[7] and signal analysis in the time/frequency domain may be used to estimate the average values of the time spent by the defect in each discrete conduction level.[8] These are usually labeled as capture time (τ_c) and emission time (τ_e), which are associated with the underlying carrier trapping and detrapping dynamics. However, when capture/emission events simultaneously occur at different defect sites, the measured signal exhibits more than two discrete levels (multi-level RTN), and the extraction of τ_c and τ_e for the different defects involved becomes increasingly complicated.

In large devices, the wider area hosts a larger count of defects distributed in space and energy, and a *1/f* noise spectrum results from the superposition of many Lorentzians,[9] each associated with the capture/emission of carriers at an individual defect. Decoding the contribution of individual defects is therefore not feasible in such structures. The observation of defect-induced RTN in smaller area devices is comparatively easier due to the lower contribution of the background thermal and white noise components. However, there are still a few inherent challenges that remain in device-level RTN analysis. These include primarily the role of the electrode, which may enhance the process-induced defect density (resulting in complex non-stationary RTN signatures) close to the metal–dielectric interface due to the

[a)]Author to whom correspondence should be addressed. Electronic mail: thamankar@sutd.edu.sg, Telephone: (+65) 9825 6723.

oxygen scavenging nature of the electrode materials (which are TiN/Ti/TaN based);[10] instrumentation limits in the standard probe station setup on the lower level of current that can be measured at a desired time resolution and the area of probing in patterned devices, which is still relatively large (20–30 nm in unit dimension even for the best case). Owing to these issues, device level RTN may not be considered as a stand-alone comprehensive technique to study the discrete defects in the dielectric from a scientific viewpoint.

While there are other techniques such as charge pumping,[11] relaxation current,[12] and stress induced leakage current (SILC) spectra[13] that have been used to study defects in different dielectric systems at the device level, they have their own limitations on the defects that are probed. Charge pumping predominantly enables detection of only interface states between the dielectric and the semiconductor, and it works well only for low leakage levels in relatively thick oxides.[11] Relaxation currents have been observed for individual defects at the device level in bias temperature instability experiments;[14,15] however, they are non-steady state signals and each defect only shows one step of jump during the relaxation process. When compared to RTN where every defect's behavior is characterized by several electron capture and emission events, relaxation currents provide very little insight into the energetics and location of the defect in action. An additional complexity with the relaxation process is the need to deconvolute the effects of charge detrapping and dielectric polarization from the measured current data.[12] SILC spectra are useful only for detection of stress induced defects when the trap-assisted tunneling component significantly exceeds the intrinsic leakage current contribution.[13] Moreover, SILC spectra lose their ability to probe multiple defects distinctly when the device area is large, and they only provide a measure of the collective effect of conduction through the network of defects that are randomly generated across the stressed oxide thin film.

To gain in depth insight into the chemical kinetics of single defects, we propose and demonstrate in this study, the possibility of using the scanning tunneling microscope (STM) for RTN analysis to study the process-induced defects/traps at a much higher spatial resolution and at sub-nano ampere range currents. The advantage of the STM-based setup is its ability to study the nature of a single defect (physical location, trap energy depth from conduction band, activation, relaxation and thermal ionization energy and trap charge state) on a blanket film at a high spatial resolution of about 10 nm, without the need for any patterned top electrode devices. STM also allows for the unique examination of defect properties at different microstructural regions (grain and grain boundary).[16] The method presented in this study will allow us to study the nature of traps in new as-deposited and annealed blanket dielectric thin films, before they are even considered for device-level implementation. Moreover, since STM analysis does not require a metal electrode, the metal–oxide interface effects do not interfere with our objective of studying the intrinsic bulk defects in the thin film of interest. However, there are certain technical limitations of the STM setup due to the "drift" of the probe tip that only allows us to reliably probe "fast traps" with time constants in the range of a few milliseconds to few tens of seconds. These advantages and limitations will be clearly evident from the experimental results presented in this study.

In order to demonstrate our hypothesis, we apply our proposed methodology to sense the noise signals in 4 nm blanket HfO_2 films. Section II describes the STM experimental setup, test conditions and materials used in our study, followed by Section III which presents the RTN characterization results. In Section IV, the time constants from the RTN signal are extracted and analyzed using robust statistical techniques to confirm the possible existence of a *meta-stable* defect state, which supports recent device level[17] and first principle studies.[18,19] A simple scientific basis for the observed results is also presented. Finally, Section V concludes the study by summarizing the key findings, documenting the challenges and advantages of the STM based noise spectroscopy approach along with proposals for further work. It is to be noted that this study only analyzes the PIT in the dielectric. The measurement conditions for the STM based RTN sensing experiments are carefully chosen so as to minimize the likelihood of generating stress induced traps.

II. DIELECTRIC CHARACTERIZATION SETUP

The sample used in our STM study consists of a 4 nm HfO_2 film deposited using atomic layer deposition (ALD) on *n*-Si (100), and further annealed at 400 °C for 40 min in an N_2 ambient resulting in a polycrystalline HfO_2 film.[20] The conditions for ALD (anneal temperature and time) are carefully chosen so as to minimize the presence of any interfacial oxide layer (SiO_x) between the HfO_2 film and Si substrate.[21,22] Analysis using XPS spectra (not shown here for brevity), *C-V* measurement (extracted material permittivity of $\kappa \sim 16$, which is close to the value for HfO_2) and *I-V* ramped sweep breakdown tests on the deposited oxide shows convincing evidence that the SiO_x layer is thinner than ~8 Å. Given the intrinsically higher trap density (N_t) in the HfO_2 layer ($N_t \sim 5.5 \times 10^{18}\,cm^{-3}$) as compared to the SiO_x layer ($N_t \sim 10^{16}\,cm^{-3}$)[23,24] and considering the size of the oxygen vacancy defect in SiO_x, which is extracted to be higher than 9 Å from percolation model based statistical breakdown analysis tests[25] (while the physical thickness here is only 8 Å), the contribution of traps residing in SiO_x can be neglected to the first order in our work here, and the voltage drop across SiO_x is also assumed to be minimal as it is not thick enough to maintain its inherent insulating property.

The experimental setup is schematically shown in Fig. 1(a). Mechanically cut Pt/Ir tips were used for the spectroscopy/RTN measurements. Once the STM tip reaches a threshold gap (z) lower than z_0, the tunneling condition is satisfied. The STM tip is then precisely positioned on the HfO_2 grain, and the tunneling current is monitored with time (*I-t*) by switching off the feedback loop. RTN signals from single or few defects can be detected using this procedure that probes the dielectric in a lateral spatial region spanning around 10 nm. We shall only consider the RTN signals measured over individual grains of the deposited HfO_2 films for this study, as these are the locations with a higher probability of accessing unclustered single defects.

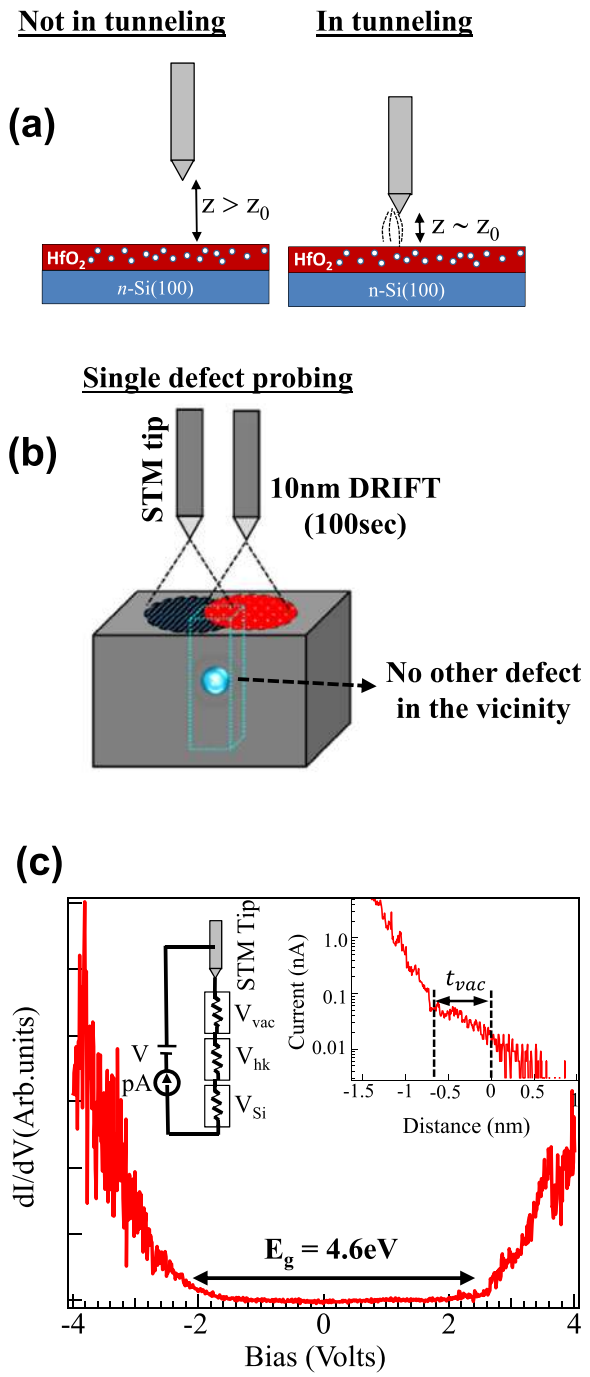

FIG. 1. Schematic diagram of the scanning tunneling microscope (STM) configuration. Only when the tip is at a distance of ($z < z_0$) is the tunneling condition satisfied. The voltage drop experienced by the dielectric is a fraction of the actual voltage applied to the tip. (b) Illustration of the possibility of detecting RTN from the same single defect with no other defect in the vicinity in spite of the inherent drift of 0.1 nm/s in the STM setup. (c) Energy gap of $E_g = 4.6$ eV, as measured using the lock-in technique ($f_0 = 2.7$ kHz and $\Delta V = 10$ mV). Inset shows a simple equivalent circuit diagram of the experiment, where V_{vac}, V_{hk} and V_{Si} represent the voltage drop across the tunnel gap, high-κ and the Si substrate, respectively. The I–z curve (also shown as an inset) is measured on an HfO_2 island (grain) to determine the vacuum gap separation (t_{vac}) used in the voltage drop calculation.

The STM setup is maintained at room temperature and ultra-high vacuum conditions ($p \sim 5 \times 10^{-10}$ mbar). As mentioned earlier, the RTN measurements were carried out with no metal–dielectric interface, thereby giving us the opportunity to probe the bulk process-induced defects in the high-κ film. The current and time resolution sensitivity offered by STM allows for the detection of single electron capture and emission events from oxygen vacancy defects. STM has been used by many groups to assess the microstructure of polycrystalline high-κ films and map the contours of the grain boundaries,[26,27] as well as for localized stressing on blanket films to assess time dependent dielectric breakdown (TDDB) resilience.[28,29] However, there are no reports of STM being used for detection of RTN signals on high-κ dielectric materials, although STM has been used successfully to detect RTN switching on SiO_2.[30] A major reason why STM is not widely applied to study RTN is due to the spatial "drift" that the tip may undergo during the measurements (typically ~0.1 nm/s), which causes the tip to move away from the defect location during the typically long duration RTN probe experiments. The drift is mainly due to the instrument mechanical perturbation and thermal gradient between the sample-tip gap, both causing the tunnel junction to vary. Given the inherent limitation due to drift in the setup, we restrict all our RTN measurements to shorter periods of time spanning less than 100 s, which corresponds to a mean shift of the tip by 10 nm (refer to Fig. 1(b)). With the STM probe area ranging between 10 and 15 nm, this is the maximum time duration for possible reliable RTN data acquisition from a single defect in spite of the change in tip location. As our results do show, stable and steady-state RTN trends at consistent current levels have been detected for time durations spanning up to 100 s. Note, however, that the drift constraint does not allow us to detect very slow traps that could have time constants in the kilo-seconds range or more, as shown by some recent reports using device level tests.[31,32]

The HfO_2 film is sensed for RTN from the process induced traps at a constant voltage bias applied to the tip (with the substrate grounded). The applied tip voltage drops across three junctions, namely, the vacuum tunnel junction (V_{vac}), the dielectric film (V_{hk}) and the Si (100) substrate (V_{Si}), as shown in the inset of Fig. 1(c). Considering that the two voltage drops are across insulators (vacuum junction and the high-κ film) and the last one is across a semiconducting substrate, we note that $V_{Si} \ll \{V_{vac}, V_{hk}\}$. For a two-layer sandwich dielectric, making use of the Gauss's law,[33] we may calculate the voltage drop across the high-κ (V_{hk}) (ignoring the very thin SiO_x interfacial layer) to be

$$V_{hk} = V_{tot}\left[\frac{\kappa_{hk} t_{vac}}{\kappa_{vac} t_{hk}} + 1\right]^{-1}, \quad (1)$$

where V_{hk} is the voltage drop across the high-κ dielectric, V_{tot} is the applied voltage to the STM tip, and $\{\kappa_{hk} = 25, \kappa_{vac} = 1\}$ represent the ideal permittivity of the high-κ and vacuum regions, respectively. The thickness of the HfO_2 film (~4 nm) and the effective thickness of the vacuum (tunnel gap) are represented by t_{hk} and t_{vac}, respectively. The spacing of the effective vacuum gap is estimated as the difference in distance between the user-defined tunnel control current [at 0 nm in the inset of Fig. 1(c)] and the sudden change in the slope of the current curve as the tip contacts the surface [at $z = -0.7$ nm in the inset of Fig. 1(c)]. Hence, in the study of our sample here, $t_{vac} \sim 0.7$ nm. Given these

values for the different material parameters and with $t_{vac} = 0.7$ nm, Eq. (1) can be used to calculate the voltage drop across the HfO_2 film to be approximately 19% of V_{tot}.

We measured the energy gap of the HfO_2 film by measuring the dI/dV curve using the lock-in technique.[34] For a 4 nm HfO_2 film, we found the energy gap to be around 4.6 eV (Fig. 1(c)), which is in good agreement with the reported bulk material bandgap values of 4.5–5.0 eV.[35,36] Prior to performing the RTN experiments, we use the dI/dV curve as a reference to set the sample bias voltage, such that adequate current can be detected across the tunnel junction. Furthermore, the bias set point is chosen such that we access only the process induced traps.

III. RTN MEASUREMENTS

From the various RTN measurements carried out at different locations across the HfO_2 film, three different characteristic trends are observed as shown in Fig. 2. The STM control current is set to 50 pA with the tip bias fixed at $V_{tot} = 3.5$ V, giving $V_{hk} \sim 3.5 \times 19\% = 0.65$ V across the 4 nm thick oxide. This corresponds to an effective ξ-field in HfO_2 of approximately $\xi = 1.66$ MV/cm. With the critical field strength (ξ_{crit}) for HfO_2 being much higher at around 5–6 MV/cm[37] and given the exponential dependence of the defect generation rate due to Hf-O bond dissociation on the ξ-field,[38] it can be confidently claimed that our RTN analysis predominantly studies PIT, keeping the probability of new stress-induced defect generation to be very low. This is all the more true given the very short measurement duration for RTN.

Note in Fig. 2 that we do not observe any monotonic gradual change in the high and low conduction levels of the RTN signals over the short period of measurement. This confirms that the impact of *x-drift* and *y-drift* is very minimal. Moreover, the magnitude of RTN fluctuation is only 3–4 times of the lowest conduction value at most. If the *z-drift* was significant, then the tunneling current should change by almost an order of magnitude for an Angstrom shift in the tunnel gap value.[39] Since this is not the case observed, the effect of *z-drift* can also be assumed to be negligible. Our RTN amplitudes (difference in current levels) range anywhere between 30 and 100 pA, which is much higher than the 5–10 pA range contribution from the background/drift induced noise.

The RTN signatures shown in Figs. 2(a)–2(c) are obtained at different locations on the same sample, and clear 2-level, 4-level, and 5-level RTN trends are observed. These RTN trends look very similar to traditional device level test patterns attributed to steady state transitions between the discrete conduction levels.[40] The 4-level and 5-level RTN signals can be viewed as a combination of the 2-level signals originating from more than one trap in a slightly more defect rich region (e.g., possibly corresponding to a defect cluster or closer in proximity to a grain boundary).

The histogram plots of the current in the inset of Figs. 2(a)–2(c) indicate the relative time spent by the RTN signal at each discrete current level during the measurement. The number of discrete levels (i.e., peaks or sub-distributions in the histogram) corresponds to a maximum of 2^N for N number of independent traps, and hence, the three different results in Figs. 2(a)–2(c) are related to the simultaneous activity of 1 trap, 2 traps, and 3 traps, respectively. If the time frame for RTN measurement was to be kept sufficiently long (which is not possible in our setup due to drift-induced constraints), then we should be able to observe an 8-level RTN signal, similar to the RTN in Fig. 2(c), due to the simultaneous activity of three distinct traps.

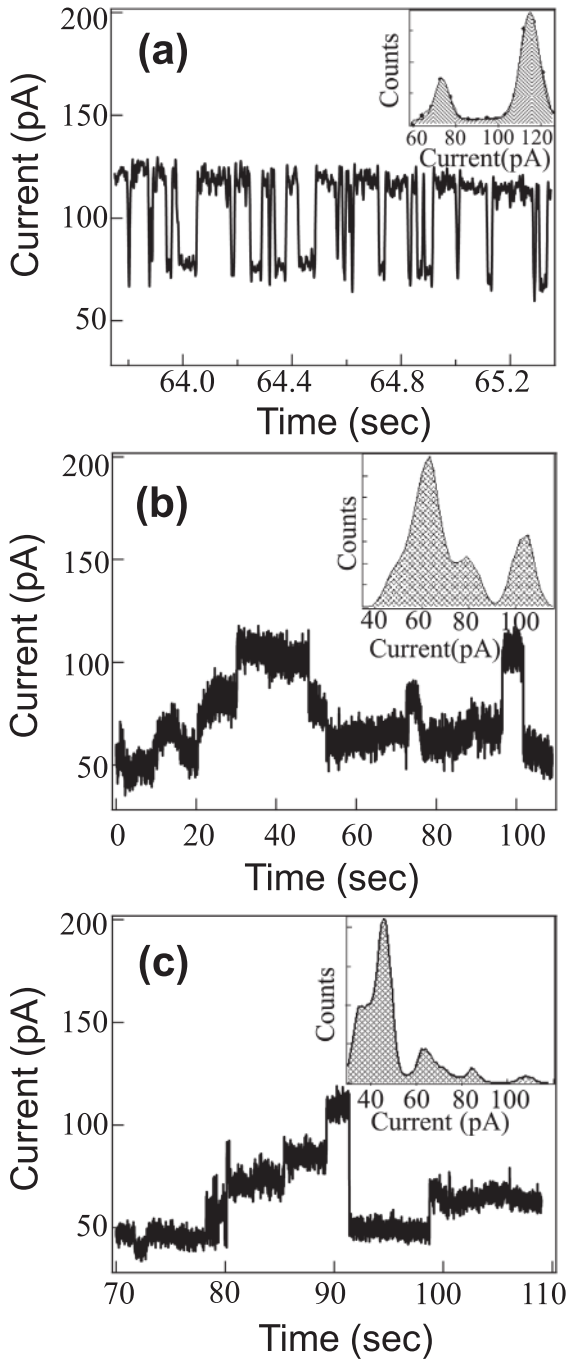

FIG. 2. (a)–(c) Various RTN signals from fast traps measured on HfO_2 at room temperature. The measurements were carried out on different HfO_2 grains, elucidating the different responses from the defects. The tunneling condition was set to a fixed value for all the measurements (3.5 V/50 pA). The insets in (a)–(c) show the histogram of the current values, from which the number of conduction levels embedded in the RTN signal can be estimated.

For further analysis, the RTN signals in the time domain can be transformed to the frequency domain to obtain the low-frequency response for these three scenarios. For example, the 2-level and 5-level RTN signals in Figs. 2(a) and 2(c) are transformed to the frequency domain as shown in Figs. 3(a) and 3(b). The power spectral density (S_I) follows a power-law trend with the frequency (f)[9] given by

$$S_I \propto \frac{1}{f^{\alpha}}. \tag{2}$$

Fitting of this empirical model to the low frequency data in the range of 1–10 Hz gives values of $\alpha \sim 1.91$ and 1.57 for Figs. 3(a) and 3(b), respectively. Ideally, a value of $\alpha \sim 2$ would correspond to a pure Lorentzian trend ($\frac{1}{f^2}$) from a single defect RTN with clear two-level current signal (with no white noise), and $\alpha \sim 1$ pertains to the $1/f$ noise due to generation-recombination of electron-hole pairs.[9] The dependence of α on the number of levels in the RTN signal (2^N) is plotted in Fig. 3(c). As the number of traps (randomly distributed in physical location and/or energy space) increases, the value of α gradually decreases. This is expected because every trap may have a different time constant in the low and high current state, corresponding to a different roll-off point in the frequency spectrum. When such noise spectra with different time constants (different roll-off points) are superimposed, the resulting signal becomes more $1/f$-like. Extrapolating the trend of α towards 1, it may be deduced that about 9–10 discrete current levels (corresponding to 2^N) are needed to observe a pure $1/f$ noise trend. This corresponds to 4 defects contributing to the RTN signal (number of defects (N) = $\log_2$(number of current levels) = $\log_2(4)$).

Another interesting feature observed in some of the RTN measurements is illustrated in the current–time data in Fig. 4(a). While the high and low current levels remain unchanged throughout, the frequency of transitions was initially "slow" from 0 to 8 s, but suddenly increased to a faster value between 8 and 12 s, before returning to the slow frequency behavior thereafter. This trend was not to be expected as there is only one trap present in the region (the RTN signal consistently has only two current levels, i.e., one trap). We speculate that this transition could correspond to the possible existence of a "metastable" state of a defect due to some temporary change in its atomic configuration or charge state. Further in-depth analysis on this signal is presented in Sec. IV.

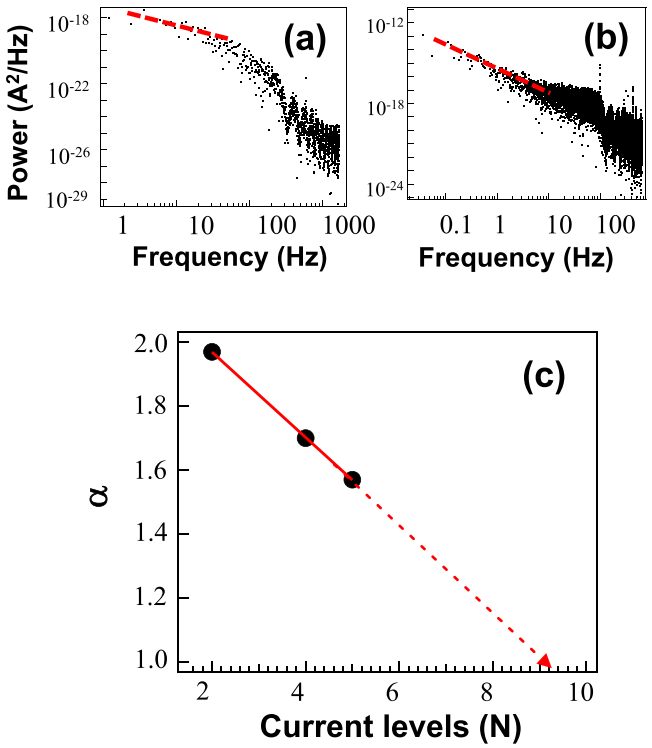

FIG. 3. (a) and (b) Power spectral density plots of the RTN signal in Figs. 2(a) and 2(c). In the low frequency regime, the value of the power law exponents, $\alpha = 1.92$ and $\alpha = 1.57$, is extracted (dashed red line). There is a gradual reduction in the exponent/slope (α) value towards 1 with increasing number of conduction levels in the steady-state RTN shown in Figs. 2(a)–2(c). Extrapolation to $\alpha = 1$ indicates that more than 3 defects are required in order to observe a $1/f$ dependence in the noise spectra.

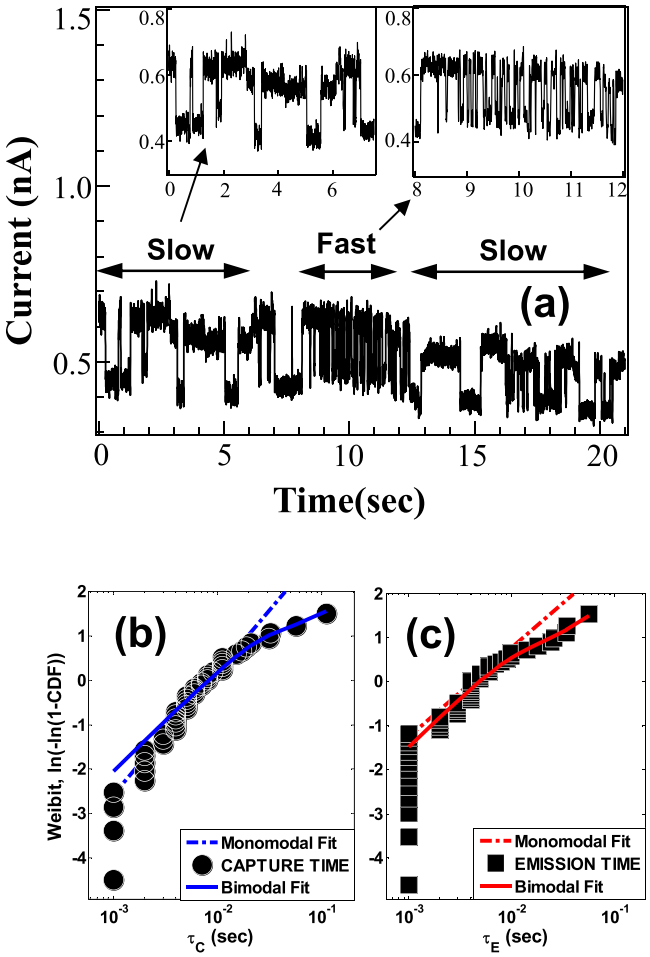

FIG. 4. (a) Metastable RTN signal from a single trap. The slow and fast RTN signals are shown in the insets. The trap exhibits "slow" transitions initially, then changes into a "fast" responding mode and followed by a "slow" response again. (b) The individual capture and emission time constants, extracted from the signal, show a bimodal trend when plotted on the exponential probability scale plot. The non-linear (bimodal) trend of the data clearly indicates the presence of two different types of response (slow and fast switching) from the same defect.

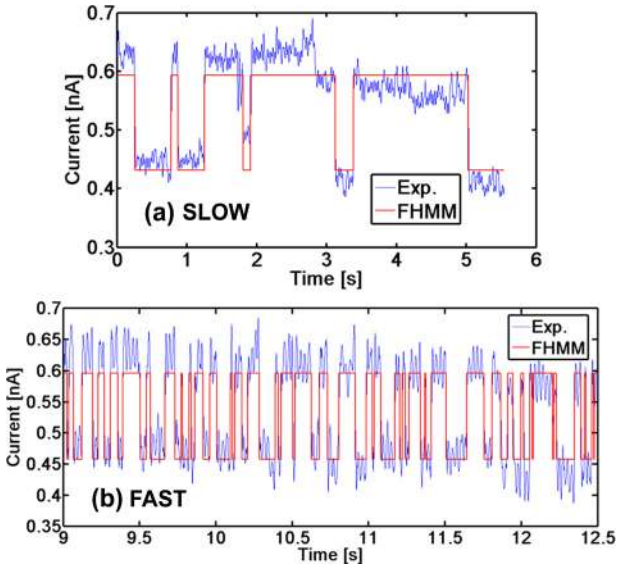

FIG. 5. (a) and (b) Resolving the bimodal RTN trends in the signal shown in Fig. 4(a). FHMM based fit (red line is the fit and blue lines represent the raw data) to the (a) "slow" and (b) "fast" phases of the trap response, corresponding to time ranges of 0–6 s and 9–12.5 s, respectively.

IV. STATISTICAL ANALYSIS OF RTN SIGNAL

To investigate the patterns in the signal of Fig. 4(a), we perform in-depth statistical analysis of the extracted time constants. For a normal two-level RTN signal, when the times for low-to-high current transition (emission time, τ_E) and high-to-low current transition (capture time, τ_C) are extracted and plotted on a probability distribution plot, they should each follow an exponential distribution with a certain mean value.[7] When the extracted time constants $\{\tau_C, \tau_E\}$ from Fig. 4(a) are plotted on a Weibit scale (equivalent to an exponential scale plot as exponential distribution is just a special case of the Weibull model with a shape parameter of 1) (Fig. 4(b)), the data show a non-linear (convexial) trend and a single distribution fit to the data (shown by the red and blue dotted straight lines in Figs. 4(b) and 4(c)) using the standard Maximum Likelihood Estimate (MLE) approach that fails to adequately represent the RTN signal observed. We then applied the mixture distribution model called the Expectation-Maximization (EM) algorithm[41] to fit a two-component exponential cumulative density function to the $\{\tau_C, \tau_E\}$ data, as represented by Eq. (3). Here ϕ represents the fraction of time constant (τ_N) data corresponding to sub-distribution (F_1), and $(1 - \phi)$ accounts for the remaining fraction which pertains to the second sub-distribution (F_2). The symbol τ_x represents the mean time constant for each sub-distribution for the capture and emission processes. When a two-distribution fit is considered, the pattern of the data is very well represented by the bimodal fit (shown by the blue and red bold curves in Fig. 4(b) and 4(c)). This bimodality confirms the existence of two different behaviors of the same trap within a single signal measured, confirming the possible presence of a metastable state for the defect.

$$F(t) = \phi \cdot F_1(t) + (1 - \phi) \cdot F_2(t),$$
$$F_x(t) = 1 - e^{-t/\tau_x}; \quad x = \{1, 2\}. \tag{3}$$

To extract the time constants corresponding to the slow and fast switching behavior of the trap, we applied the Factorial Hidden Markov Model (FHMM),[42] which is an effective algorithm that enables the decoding of any multi-level RTN signal into its independent two-level components, estimating the distributions of both τ_C and τ_E, and analyzing each (exponential) distribution separately to extract the values of $(\tau_C, \tau_E)_{slow}$ and $(\tau_C, \tau_E)_{fast}$. Figs. 5(a) and 5(b) show the slow and fast switching portion of the RTN signal analyzed using the FHMM technique. The results of the FHMM include the extraction of the magnitude of the switching current (shown by the red line fit to the measured data) as well as the $\{\tau_C, \tau_E\}$ values. When the data are extracted for $(\tau_C, \tau_E)_{slow}$ in Figs. 6(a) and 6(c) and for $(\tau_C, \tau_E)_{fast}$ in Figs. 6(b) and 6(d) separately on an exponential probability scale, all the data sets show a very good linear fit implying that they constitute part of a unique steady-state RTN behavior of the trap. These exponential plots provide further confirmation of the existence of a metastable state of the trap that produced the RTN signal. The extracted mean values for the time constants are $(\tau_C)_{slow} \sim 846$ m-s, $(\tau_E)_{slow} \sim 314$ m-s, $(\tau_C)_{fast} \sim 56$ m-s, and $(\tau_E)_{fast} \sim 39$ m-s.

The physical phenomena underlying the temporary metastable transition of the trap is still not well understood and needs further atomistic insight. Several recent experimental

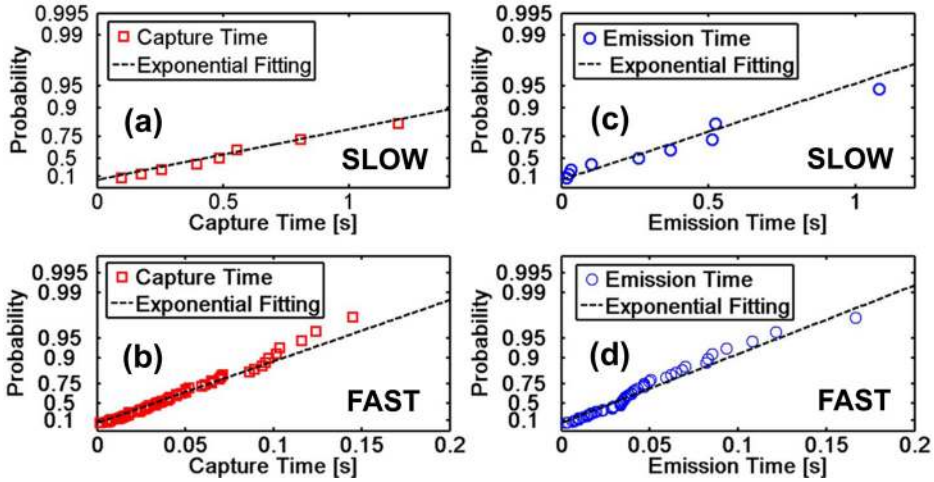

FIG. 6. Capture (a) and (b) and emission (c) and (d) time constants of the "slow" (a) and (c) and "fast" (b) and (d) components of the RTN signal are plotted separately on an exponential probability plot showing clear monomodal trends. The mean values of the time constants for the regular and metastable states of the single trap can be deduced from this plot. The dotted lines represent the best fit trend to the data using the maximum likelihood estimate (MLE) algorithm.

studies have confirmed the possible metastable nature of the oxygen vacancy defect in HfO_2.[43,44] One plausible explanation provided is that the trap undergoes a configurational change due to either charge exchange with the underlying substrate or structural relaxation during the capture/emission process.[45] As a result, the defects can have more than two states responsible for the RTN signal. This, along with the multi-phonon mechanism, which involves lattice relaxation and rearrangement around the defect caused by the Coulomb coupling between the neighboring lattice ions and the charge trapped vacancies, can explain the complex trap dynamics that we observe.[46,47] Recently, a different approach was also proposed which models the RTN as a convoluted effect of the electrostatic interactions between the V_O defects and the charge carriers trapped at defects of different nature (e.g., oxygen ions), which may exhibit relatively slow trapping/de-trapping dynamics, in agreement with the observed RTN timing.[17] In this framework, the temporary alteration of the RTN properties (as shown in Fig. 4 (a)) may be related to the movement of such additional defects between neighboring positions (e.g., interstitial jumps) under the action of the applied field. This would indeed change the trapping/de-trapping dynamics of this additional defect and, consequently, the statistical properties of the RTN signal. While previous reports and claims on the metastable state of the oxygen vacancy defect in HfO_2 are based mostly on first principle simulations[48–50] or device level noise measurements,[43,44] our approach of proving its existence relies on the use of concrete statistical methods to demonstrate the highly bimodal nature of the time constant distributions within a single RTN signal representing the response of a single defect.

V. CONCLUSIONS

In this study, steady-state RTN signals for fast traps in HfO_2 thin films were observed using STM at the nanoscale. For the short durations of measurement, the drift effect from the STM tip was shown to be negligible. The approach enabled detection of the RTN signal at a very confined area of $\sim 10\,\text{nm} \times 10\,\text{nm}$ in size and allowed us to probe individual process-induced defects in blanket thin films. We observed different noise responses depending on the number of traps in the dielectric region of interest under the tip and also demonstrated the possible existence of metastable oxygen vacancy defect states with temporary and reversible RTN properties, although the physical origin of this change is not elucidated in detail here and warrants further atomistic studies.

The STM-based localized RTN probing method could be used to address a variety of important issues in defect analysis of high-κ films. The methodology can be effectively applied for process qualification, variability analysis and optimization of the dielectric deposition recipe in a commercial manufacturing line by extracting the number density and spatial distribution of process-induced traps (fast traps). Given the atomic scale sensitivity of the STM, we should be able to probe the RTN behavior of defects that are located either inside the grain or along the grain boundary. A comparison of the RTN signals at the grain and grain boundary locations of polycrystalline HfO_2 films will be particularly useful in revealing the different defect energy levels arising from the different local atomic arrangements. Bias voltage-dependent RTN analysis using STM, with suitable modeling, could also be carried out to extract further details on the trap depth and physical location of every defect in the dielectric thin film. Finally, one of the complexities that remain to be addressed in the future is the spatial field distribution in the dielectric arising from the STM tip. We expect the flux line patterns to be non-uniform, as the STM tip is just a few nanometers in size (high curvature) and a drastic change in the field distribution may exist over a few tens of nanometer region. The presence of multi-layer dielectrics and interfacial oxides can further complicate the field distribution patterns that will certainly impact the RTN trends measured.

ACKNOWLEDGMENTS

The authors acknowledge the funding support under the SUTD-ZJU research collaboration grant (ZJURP1300104). R. Thamankar acknowledges the support of the Institute of Materials Research and Engineering (IMRE), *A*STAR*, Singapore for access to the STM facility.

[1]K. Torri, H. Kitajima, T. Arikado, K. Shiraishi, S. Miyazaki *et al.*, "Physical model of BTI, TDDB and SILC in HfO_2-based high-κ gate dielectrics," IEEE Int. Electron Devices Meet. **2004**, 129–132 (2004).
[2]X. Wu, D. B. Migas, X. Li, M. Bosman, N. Raghavan, V. E. Borisenko, and K. L. Pey, "Role of oxygen vacancies in HfO_2-based gate stack breakdown," Appl. Phys. Lett. **96**(17), 172901 (2010).
[3]J. P. Campbell, J. Qin, K. P. Cheung, L. C. Yu, J. S. Suehle, A. Oates, and K. Sheng, "Random telegraph noise in highly scaled nMOSFETs," in *Proceedings of the 2009 IEEE International Reliability Physics Symposium* (2009), pp. 382–388.
[4]C. M. Chang, S. S. Chung, Y. S. Hsieh, L. W. Cheng, C. T. Tsai, G. H. Ma, S. C. Chien, and S. W. Sun, "The observation of trapping and detrapping effects in high-κ gate dielectric MOSFETs by a new gate current random telegraph noise (I_G-RTN) approach," IEEE Int. Electron Devices Meet. **2008**, 1–4 (2008).
[5]Y. H. Tseng, W. C. Shen, C. E. Huang, C. J. Lin, and Y. C. King, "Electron trapping effect on the switching behavior of contact RRAM devices through random telegraph noise analysis," IEEE Int. Electron Devices Meet. **2010**, 28.5.1–28.5.4 (2010).
[6]M. J. Uren, M. J. Kirton, and S. Collins, "Anomalous telegraph noise in small-area silicon metal-oxide-semiconductor field-effect transistors," Phys. Rev. B **37**(14), 8346–8350 (1988).
[7]K. Abe, A. Teramoto, S. Sugawa, and T. Ohmi, "Understanding of traps causing random telegraph noise based on experimentally extracted time constants and amplitude," in *Proceedings of the IEEE International* Reliability Physics Symposium (IRPS) (2011), p. 4A.4.1.
[8]R. Gusmeroli, C. M. Compagnoni, A. Riva, A. S. Spinelli, A. L. Lacaita, M. Bonanomi, and A. Visconti, "Defects spectroscopy in SiO_2 by statistical random telegraph noise analysis," IEEE Int. Electron Devices Meet. **2006**, 1–4 (2006).
[9]M. Von Haartman and M. Östling, *Low-Frequency Noise in Advanced MOS Devices* (Springer Science & Business Media, 2007).
[10]H. Y. Lee, P. S. Chen, T. Y. Wu, Y. S. Che, C. C. Wan, P. J. Tzen, C. H. Lin, F. Chen, C. H. Lien, and M. J. Tsai, "Low power and high speed bipolar switching with a thin reactive Ti buffer layer in robust HfO_2 based RRAM," IEEE Int. Electron Devices Meet. **2008**, 1–4 (2008).
[11]J. T. Ryan, J. Zou, R. Southwick, J. P. Campbell, K. P. Cheung, A. S. Oates, and R. Huang, "Frequency-modulated charge pumping with extremely high gate leakage," IEEE Trans. Electron Devices **62**(3), 769–775 (2015).
[12]C. H. Yang, Y. Kuo, and C. H. Lin, "Charge detrapping and dielectric breakdown of nanocrystalline zinc oxide embedded zirconium-doped hafnium oxide high-k dielectrics for nonvolatile memories," Appl. Phys. Lett. **96**, 192106 (2010).

[13]R. O. Connor, L. Pantisano, R. Degraeve, T. Kauerauf, B. Kaczer, P. J. Roussel, and G. Groeseneken, "SILC defect generation spectroscopy in HfSiON using constant voltage stress and substrate hot electron injection," in *Proceedings of the* IRPS *2008 IEEE International* Reliability Physics Symposium (2008), pp. 324–329.
[14]M. T. Luque, R. Degraeve, P. J. Roussel, L. A. Ragnarsson, T. Chiarella, N. Horiguchi, A. Mocuta, and A. Thean, "Fast ramped voltage characterization of single trap bias and temperature impact on time-dependent variability," IEEE Trans. Electron Devices **61**(9), 3139–3144 (2014).
[15]S. M. Amoroso, L. Gerrer, F. Adamu-Lema, S. Markov, and A. Asenov, "Statistical study of bias temperature instabilities by means of 3D 'atomistic' simulation," in *Bias Temperature Instability for Devices and Circuits* (Springer, New York, 2014), pp. 323–348.
[16]K. S. Yew, D. S. Ang, L. J. Tang, K. Cui, G. Bersuker, and P. S. Lysaght, "Scanning tunneling microscopy study of the multi-step deposited and annealed $HfSiO_x$ gate dielectric," J. Electrochem. Soc. **158**(10), H1021–H1026 (2011).
[17]F. M. Puglisi, P. Pavan, L. Vandelli, A. Padovani, M. Bertocchi, and L. Larcher, "A microscopic physical description of RTN current fluctuations in HfO_x RRAM," in *Proceedings of the 2015 IEEE International* Reliability Physics Symposium (IRPS) (2015), pp. 5B.5.1–5B.5.6.
[18]E. Choi and K. J. Chang, "Charge-transition levels of oxygen vacancy as the origin of device instability in HfO_2 gate stacks through quasiparticle energy calculations," Appl. Phys. Lett. **94**, 122901 (2009).
[19]Y. Guo and J. Robertson, "Oxygen vacancy defects in Ta_2O_5 showing long-range atomic re-arrangements," Appl. Phys. Lett. **104**(11), 112906 (2014).
[20]K. Shubhakar, K. L. Pey, N. Raghavan, S. S. Kushvaha, M. Bosman, Z. R. Wang, and S. J. O'Shea, Microelectron. Eng. **109**, 364–369 (2013).
[21]P. G. M. Gonzalez, M. O. Vazquez, and A. H. Gomez, "Aperture-time of oxygen-precursor for minimum silicon incorporation into the interface-layer in atomic layer deposition-grown HfO_2/Si nanofilms," J. Vac. Sci. Technol. A **33**, 010602 (2015).
[22]P. G. M. Gonzalez, M. O. Vazquez, F. E. Magaña, and A. H. Gomez, "Interface layer in hafnia/Si films as a function of ALD cycles," J. Vac. Sci. Technol. A **31**, 010601 (2013).
[23]O. Pirrotta, L. Larcher, M. Lanza, A. Padovani, M. Porti, M. Nafria, and G. Bersuker, "Leakage current through the poly-crystalline HfO_2: Trap densities at grains and grain boundaries," J. Appl. Phys. **114**, 134503 (2013).
[24]J. Molina and R. Thamankar, "Performance of ultra-thin HfO_2-based MIM devices after oxygen modulation and post-metallization annealing in N_2," Phys. Status Solidi A (submitted).
[25]C. H. Chen, I. Y. K. Chang, J. Y. M. Lee, F. C. Chiu, Y. K. Chiouand, and T. B. Wu, "Reliability properties of metal oxide semiconductor capacitors using HfO_2 high-κ dielectric," Appl. Phys. Lett. **91**, 123507 (2007).
[26]G. Bersuker, J. Yum, L. Vandelli, A. Padovani, L. Larcher, V. Iglesias, M. Porti *et al.*, "Grain boundary-driven leakage path formation in HfO_2 dielectrics," Solid-State Electron. **65**, 146–150 (2011).
[27]V. Iglesias, M. Lanza, K. Zhang, A. Bayerl, M. Porti, M. Nafria, X. Aymerich, G. Benstetter, Z. Y. Shen, and G. Bersuker, "Degradation of polycrystalline HfO_2-based gate dielectrics under nanoscale electrical stress," Appl. Phys. Lett. **99**(10), 103510 (2011).
[28]K. S. Yew, D. S. Ang, and G. Bersuker, "Bimodal Weibull distribution of metal/high-κ gate stack TDDB—Insights by scanning tunneling microscopy," IEEE Electron Device Lett. **33**(2), 146–148 (2012).
[29]R. Foissac, S. Blonkowski, M. Kogelschatz, P. Delcroix, M. Gros-Jean, and F. Bassani, "Impact of bilayer character on high-κ gate stack dielectrics breakdown obtained by conductive atomic force microscopy," Microelectron. Reliab. **53**(12), 1857–1862 (2013).
[30]M. E. Welland and R. H. Koch, "Spatial location of electron trapping defects on silicon by scanning tunneling microscopy," Appl. Phys. Lett. **48**, 724–726 (1986).
[31]G. Rzepa, M. Waltl, W. Goes, B. Kaczer, and T. Grasser, "Microscopic oxide defects causing BTI, RTN, and SILC on high-κ FinFETs," in *Proceedings of the 2015 International Conference on Simulation of Semiconductor Processes and Devices (SISPAD)* (2015), pp. 144–147.
[32]T. Grasser, H. Reisinger, W. Goes, T. Aichinger, P. Hehenberger, P. J. Wagner, M. Nelhiebel, J. Franco, and B. Kaczer, "Switching oxide traps as the missing link between negative bias temperature instability and random telegraph noise," IEEE Int. Electron Devices Meet. **2009**, 1–4 (2009).
[33]M. Houssa, *High-κ Gate Dielectrics* (Institute of Physics, Bristol, 2004).
[34]W. J. Kaiser and R. C. Jaklevic, "Scanning tunneling microscopy study of metals: spectroscopy and topography," Surf. Sci. **181**, 55–68 (1987).
[35]J. Aarik, H. Mändar, M. Kirm, and L. Pung, "Optical characterization of HfO_2 thin films grown by atomic layer deposition," Thin Solid Films **466**(1), 41–47 (2004).
[36]G. D. Wilk, R. M. Wallace, and J. M. Anthony, "High-κ gate dielectrics: Current status and materials properties considerations," J. Appl. Phys. **89**, 5243–5275 (2001).
[37]J. McPherson, J. Y. Kim, A. Shanware, and H. Mogul, "Thermochemical description of dielectric breakdown in high dielectric constant materials," Appl. Phys. Lett. **82**(13), 2121–2123 (2003).
[38]G. Bersuker, Y. Jeon, and H. R. Huff, "Degradation of thin oxides during electrical stress," Microelectron. Reliab. **41**(12), 1923–1931 (2001).
[39]D. A. Bonnell and B. D. Huey, "Basic principles of scanning probe microscopy," in *Scanning probe Microscopy and Spectroscopy: Theory, Techniques, and Applications*, 2nd ed. (Wiley-VCH, New York, 2001).
[40]S. S. Chung and C. M. Chang, "The investigation of capture/emission mechanism in high-κ gate dielectric soft breakdown by gate current random telegraph noise approach," Appl. Phys. Lett. **93**, 213502 (2008).
[41]S. Jiang and D. Kececioglu, "Maximum likelihood estimates, from censored data, for mixed-Weibull distributions," IEEE Trans. Reliab. **41**(2), 248–255 (1992).
[42]F. M. Puglisi and P. Pavan, "Factorial hidden Markov model analysis of random telegraph noise in resistive random access memories," ECTI Trans. Electr. Eng., Electron. Commun. **12**(1), 24–29 (2014).
[43]J. Jingwei, Y. Qiu, S. Guo, R. Wang, P. Ren, P. Hao, and R. Huang, "New Framework for the random charging/discharging of oxide traps in HfO_2 gate dielectric: *Ab-initio* simulation and experimental evidence," IEEE Int. Electron Devices Meet. **2014**, 21.4.1–21.4.4 (2014).
[44]C. H. Scott, Y. J. Huang, S. S. Chung, H. Y. Lee, Y. S. Chen, F. T. Chen, P. Y. Gu, and M. J. Tsai, "New observations on the regular and irregular noise behavior in a resistance random access memory," in *Proceedings of the IEEE Integrated Reliability Workshop (IIRW)* (2014), pp. 94–98.
[45]W. Goes, M. Waltl, Y. Wimmer, G. Rzepa, and T. Grasser, "Advanced modeling of charge trapping: RTN, *1/f* noise, SILC, and BTI," in *Proceedings of the IEEE International Conference on Simulation of Semiconductor Processes and Devices (SISPAD)* (2014), pp. 77–80.
[46]T. Grasser, "Stochastic charge trapping in oxides: From random telegraph noise to bias temperature instabilities," Microelectron. Reliab. **52**(1), 39–70 (2012).
[47]D. Veksler, G. Bersuker, A. Koudymov, C. D. Young, M. Liehr, and B. Taylor, "Comprehensive analysis of charge pumping data for trap identification," in *Proceedings of the IEEE International Reliability Physics Symposium (IRPS)* (2011), p. GD-4.
[48]D. M. Fleetwood, "*1/f* noise and defects in microelectronic materials and devices," IEEE Trans. Nucl. Sci. **62**(4), 1462–1486 (2015).
[49]K. P. McKenna and D. M. Ramo, "Electronic and magnetic properties of the cation vacancy defect in *m*-HfO_2," Phys. Rev. B **92**, 205124 (2015).
[50]Y. Qiu, R. Wang, J. Ji, and R. Huang, "Deep understanding of oxide defects for stochastic charging in nanoscale MOSFETs," in *Proceedings of the IEEE Silicon Nanoelectronics Workshop (SNW)* (2014), pp. 1–2.